Review of "Two different phytoplankton blooming mechanisms over the East China Sea during El-Niño decaying summers" by Lee et al.

Comment on egusphere-2024-3406 | Anonymous Referee #3:

General Comments:

The study uses satellite remote sensing, reanalysis data, and model simulation to investigate two mechanisms (river discharge and upwelling) behind how ENSO cycle influences phytoplankton biomass in East China Sea, an area of fisheries and biogeochemical importances, nd is subjected to anthropogenic perturbations.

Response: We appreciate reviewer #3's helpful comments and valuable suggestions. We have revised the manuscript by fully incorporating the reviewer's comments. Our responses to the specific comments are as follows:

• The authors conclude that both mechanisms are relevant to the positive surface Chl a anomalies during ENSO phase based mainly on correlation analysis. However, correlation does not mean causality. If you rely on correlation analysis, the correlation between nutrient fluxes (horizontal transport or vertical transport) and Chl a under variable phases of ENSO cycle may be more robust.

Response: We appreciate Referee#3's suggestion. We have newly incorporated the contribution of nutrient supply through the Taiwan Strait (TS) to the anomalous increases in Surface Chlorophyll-a (SCHL) concentrations in the East China Sea (ECS) during the summer following the El Niño's events (Chen et al., 2015; Huang et al., 2015; Zhang et al., 2015). In the revised manuscript, we have extensively addressed this by incorporating the nutrient transport mechanism through the TS (TS-transport-driven mechanism). Using nutrient data from CMEMS reanalysis and current data from Simple Ocean Data Assimilation (SODA) reanalysis, we calculated the meridional

phosphate (PO_4) transport during the summers of El Niño's decaying phase (refer to “Data and Method” for details). Our findings reveal a markedly strong PO_4 transport through the TS, highlighting its critical role in driving phytoplankton blooms in the ECS (Figure R1, we added Figure R1a as Figure 1d to the revised manuscript).

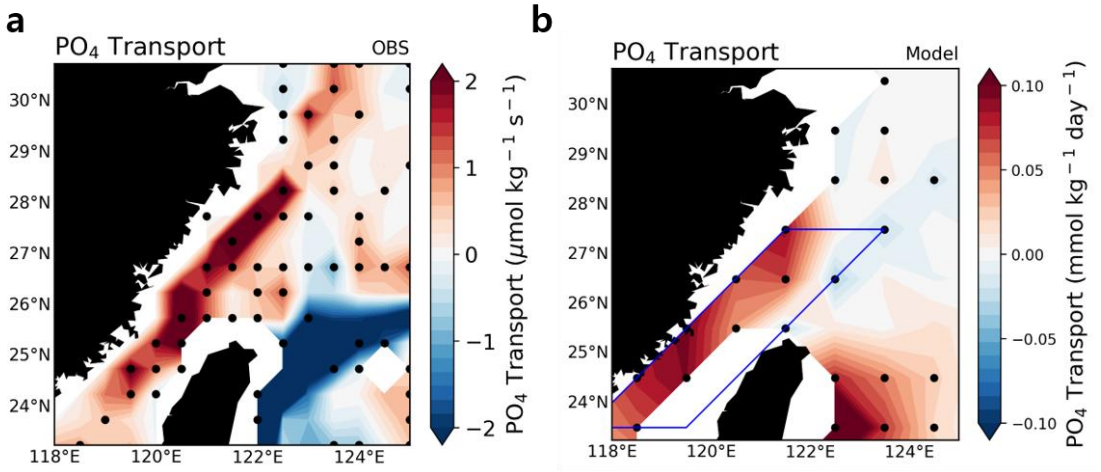

Figure R1. Composite map of meridional PO_4 transport anomalies during El Niño decaying summer season in the Taiwan Strait (TS) for all El Niño cases in observations (Left Panel) and model results (Right Panel). All the black dots where the responses are statistically significant at the 90% (in obseravtions) and 95% (in model results) confidence level, determined using the bootstrap method.

In addition, the model results demonstrate that the correlation between runoff (r = 0.59**; Figure R2a) and SCHL is weaker compared to the correlation between meridional PO_4 transport through the TS (represented as the blue diagonal box in Figure R2b) and SCHL (r = 0.68**; Figure R2b). In addition to the TS region, the meridional PO_4 transport flux in longitudinal line and SCHL correlations at 26.5°N (120.5°E–122.5°E) and 27.5°N (121.5°E–123.5°E) also exhibit significantly high positive correlations of 0.66 and 0.57, respectively (Figure R3). Moreover, the distinction between the strong blooming and non-blooming groups reveals a pronounced difference in the magnitude of meridional PO_4 transport through the TS

(Figure R4). We have incorporated Figure R2b and Figure R4 as Figure 6 in the main text. Therefore, we have added a paragraph to the main text to describe the TS-transport-driven blooming mechanism based on the model results:

(L256-265): We also investigated the TS-transport-driven blooming mechanism, which is well known for its significant role in nutrient supply through the TS. We analyzed the meridional PO_4 transport by comparing two groups as the same as Figure 5, and found remarkably distinct differences between them (Figure 6a-c). Notably, within the TS, a strong positive (negative) signal was identified in the SB (NB) group. For the SB group, the nutrient flux exhibited a significant positive signal reaching the target region, potentially supplying large amount of nutrient and making a substantial contribution to SCHL blooming in the ECS region. Furthermore, a positive correlation of 0.68—higher than the runoff-driven mechanism—was identified between the anomalous SCHL blooming magnitude in the target region and meridional PO_4 transport index indicated by the blue diagonal box in the TS region (Figure. 6d). This underscores the critical role of the TS-transport-driven mechanism in fostering nutrient into the ECS region.

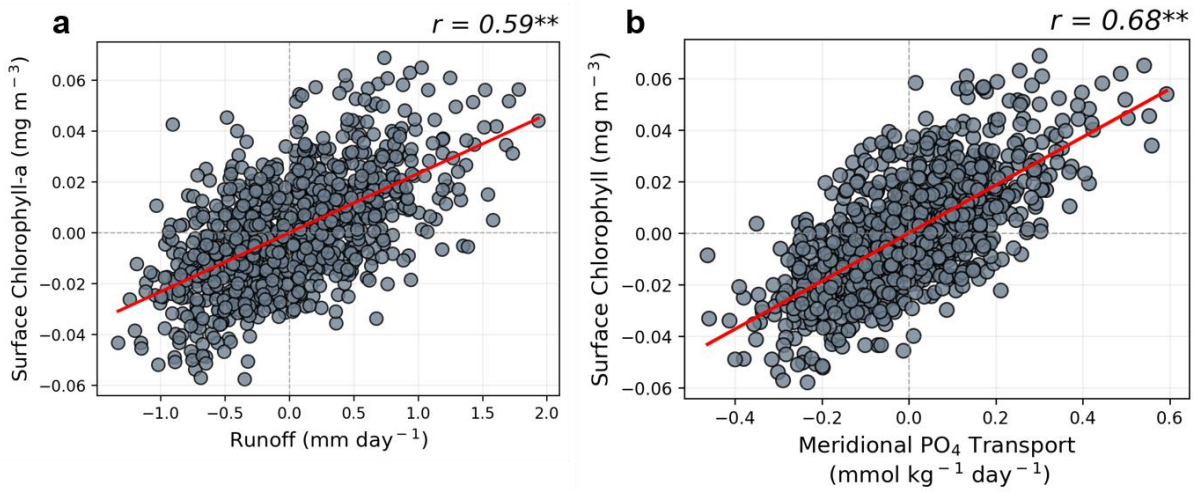

Figure R2. **(a)** The relationship between area-averaged runoff and SCHL anomalies over the target region , and **(b)** the relationship between area-averaged meiridonal PO_4 transport and SCHL anomalies over the target region.

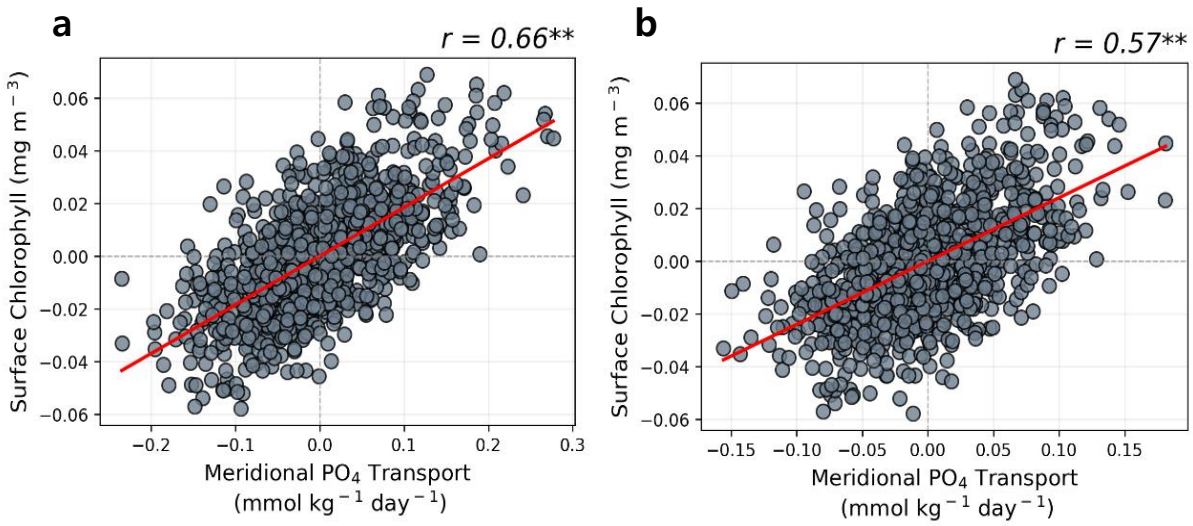

Figure R3. The relationship between zonally-averaged meridional PO4 transport (26.5˚N-120.5˚E-122.5˚E; Left Panel / 27.5˚N – 121.5˚E-123.5˚E; Right Panel) and SCHL anomalies over the target region.

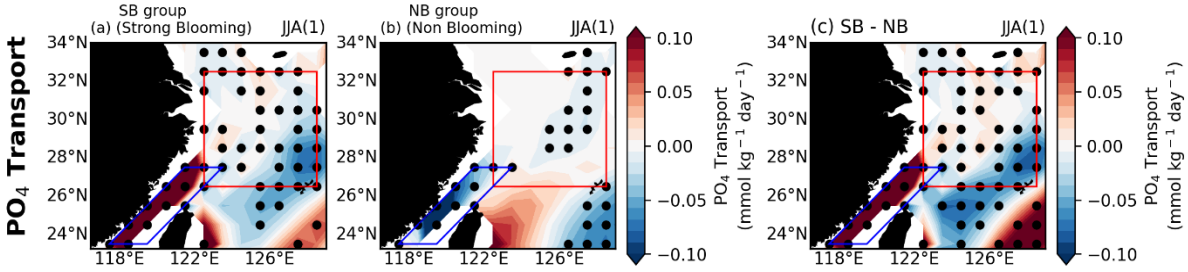

Figure R4. Composite maps of meridional PO_4 transport anomalies during El Niño decaying summer for **(a)** Strong Blooming group, **(b)** Non-Blooming group and the **(c)** difference between the two groups.

In response to the reviewer's comment, we calculated a monthly correlation of meridional PO_4 transport along a zonally averaged longitudinal line near the TS. This approach was employed to more robustly evaluate the influence of nutrient flux through the TS on SCHL over the ECS region during the variable ENSO cycle. Both observational data and model results reveal that the correlation is strongest during the summer season (Figure R5). This seasonal analysis underscores the significant role of PO_4 transport through the TS in influencing phytoplankton blooms in the ECS

especially during the summer season.

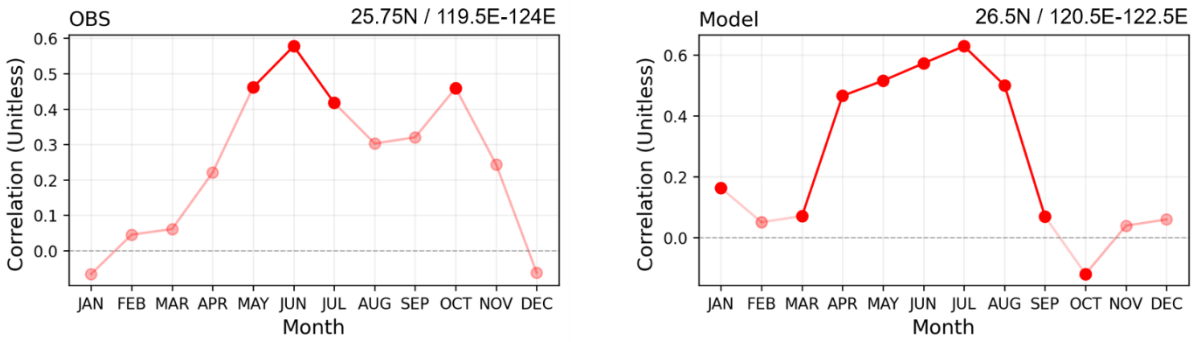

Figure R5. The plots indicate the seasonal variation of correlation coefficient between surface chlorophyll-a (SCHL) during summer season (June-July-August; JJA) in the target region and monthly meridional PO_4 transport in Taiwan Strait (TS) by zonally-averaged at specific latitude (OBS : 25.75˚N / 119.5˚E-124˚E; Model : 26.5˚N / 120.5˚E-122.5˚E) in both **(a)** reanalysis data and **(b)** model. The deeper red colors indicate that the p-value is below 0.05, signifying statistical significance at the 95% confidence level.

We also have revised the title of the manuscript to **"Phytoplankton Blooming Mechanisms over the East China Sea during El Niño Decaying Summers"** to better reflect the scope and findings of our study.

Furthermore, we have added the description that the runoff-driven mechanism encompasses nutrient input resulting from the entrainment of subsurface waters via buoyancy upwelling by following another referee's comment as follows:

(L139-145): In addition to the direct riverine nutrient input, enhanced river discharge can facilitate nutrients to the ECS region through buoyancy upwelling (Chen, 2008; Chen et al., 2003; Chen, 2000; Hill, 1998). When the out-flowing river plume becomes more substantial than the incoming river discharge, subsurface waters are readily upwelled to preserve the water balance. Consequently, the nutrient-rich Kuroshio subsurface waters ascend along the ECS shelf edge, providing essential nutrients. This buoyancy-driven upwelling occurs

independently of wind conditions, driven primarily by the physical properties of the subsurface waters in response to the intensified river outflow.

(L170-174): Although the GFDL-CM2.1 ESM does not simulate P inputs from riverine inflows, it does account for P supply through the dynamic ascent of subsurface waters driven by buoyancy upwelling resulting from river discharge. Therefore, beyond analyses based on observational and reanalysis data, long-term model simulations enable us to comprehensively understand the phytoplankton blooming mechanisms in the ECS during the following summers of El Niño events.

Therefore, we believe the extensively revised manuscript offers a more comprehensive understanding of the mechanisms driving phytoplankton blooming in the ECS during El Niño decaying summers.

• The main weakness of this study is the coarse resolution of the model used. With 1° by 1° resolution, mesoscale processes related to river discharge may not be resolved. In fact, the model failed to reproduce the distribution of Chl anomalies of ECS as observed in remote sensing (compare Figure 1a and Figure 3a). The modeled Chl distribution pattern is more related to Taiwan Strait Current from the south than due to river plume. Does the model sufficiently simulate the observed nutrient distributions?

Response: We thanks for the referee's valuable comments about the reliability of the model simulations.

We agree with the reviewer that the Earth System Model (ESM) used in our study has a relatively coarse resolution of 1° × 1°. However, our analyses indicate that the mechanisms reported in observational studies are sufficiently replicated in the

model results. Therefore, we believe that the coarse resolution model is also somewhat capable of simulating the mechanisms elucidated in our study.

Furthermore, satellite data tend to overestimate SCHL values near river estuary due to turbidity, as reported by Yamaguchi *et al* (2012). In addition, the GFDL-CM2.1 model used in our study does not simulate phosphate inflow from river discharge, which can lead to an underestimation of SCHL anomalies compared to satellite data.

Dunne *et al* 2013 showed the bias of biogeochemical variables (NO_3, PO_4, Chlorophyll-a) using both GFDL-ESM2M (z-coordinate model) and GFDL-ESM2G (isopycnal-coordinate model) models compared to observations. For nutrients (NO_3, PO_4), both models exhibited a high spatial variance captured coefficient ($r^2 > 0.8$), indicating effective replication of global spatial patterns. In the ECS, the model underestimated nitrate (NO_3) input from river runoff, resulting in an underestimation of nutrient concentrations near the Yangtze River estuary (YRE; Figure R6a). Model simulation is improved as the distance from the estuary increases. The model does not simulate the riverine input of PO4, which leads to a slight underestimation of PO_4 concentrations from the YRE to the Bohai Sea (Figure R6b). Similar to NO_3, the model's accuracy for PO_4 improved notably in offshore areas.

However, our model successfully replicates phytoplankton blooms in the ECS region, driven by nutrient inputs from river discharge, and additional nutrient transport through the TS as reported in observational studies. Furthermore, we identified that both runoff- and TS-transport-driven mechanisms are the primary contributors and confirmed that their spatial contributions are well reproduced, aligning with previous studies. Therefore, we believe that the model’s resolution does not significantly impact the validity of our study.s

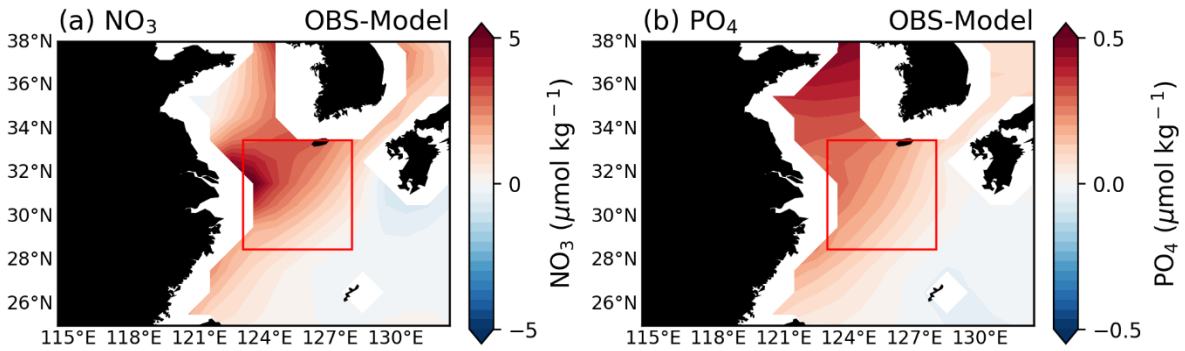

Figure R6. Annual bias between observed and modeled **(a)** NO_3 and **(b)** PO_4 concentrations.

• The authors stated that phosphate input from river was not considered in the model, however within the Yangtze river estuary, there is a positive correlation between P and Chl (Figure 2c), that is, the Chl is stimulated by other water masses rich in phosphate. This can't be explained by increasing river water discharge, as Yangtze river water is high in N/P ratio in reality, and not included in the model. There are reports showing phosphate rich water with low N/P ratio is originated from Taiwan Strait Current (Huang et al., 2019). Therefore, the model might be simulating the straightening Taiwan Strait Current during ENSO phase, assuming the model represents the N/P correctly.

Response: We thank to the referee for the valuable comments regarding the nutrient sources in the ECS region.

As we responsed above, we have substantially re-organized the manuscript. Initially, our study focused on the runoff-driven mechanism and the additional role of the upwelling-driven mechanism. However, we have now revised this manuscript to state the combined roles of the runoff-driven and TS-transport-driven mechanisms, with suggesting the additional role of upwelling-driven mechanism. This substantial reorganization enhances the clarity and value of our study, providing a more clear understanding of the mechanism influencing phytoplankton blooms in the ECS region.

Another caveat of simulating the Chl using plankton ecosystem model coupled with ocean GCM is that top-down control is not considered in majority of the models. Under same nutrient supply, Chl a may increase if grazers are suppressed by grazing of upper trophic levels.

As noted by the referee, the TOPAZ ecosystem model simulates the grazing rate by upper-level predators (Dunne et al., 2010). In this model, phytoplankton is detailed into three categories: large phytoplankton, small phytoplankton, and diazotroph phytoplankton. The grazing terms for small phytoplankton and diazotroph phytoplankton are simulated to increase proportionally to the 2nd power of their concentrations, while for large phytoplankton, the grazing rate increases proportionally to the 4/3 power of their concentration. Therefore, the grazing term driven by upper-level predators is inherently proportional to the chlorophyll-a concentration.

• The descriptions in the Data and Methods are in sufficient. It is not quite clear to me what the exact time frame of the analysis in this study. Line 65-66 stated 25 years of remote sensing data were used, does that mean the same time period is covered in model and re-analysis data? But in Figure 3, the figure legend mentioned 176 years of El Nino cases in ESM were analyzed. Some statistical analysis such as “joint composition analysis” may not be familiar to readers, me included, a reference should be very helpful.

Response: In our study, we utilized observational and reanalysis data spanning a 25-year period (1998–2022). To compensate for the relatively short duration and limitation of the datasets, we analyzed long-term simulation (1,000 years) under the present-day climate condition using GFDL-CM2.1. Using these 1,000-year simulations, we identified 176 El Niño cases, enabling a comprehensive analysis of the mechanisms driving chlorophyll blooming in the East China Sea during the El Niño decaying summer season using diverse El Niño cases. To provide additional

clarification regarding the available period of model data, we have added the description to the "Data and Method" section as follows:

(L94-97): We used the present climate-based (1990-year atmospheric CO_2 concentration level; 353 parts per million (ppm)) long-term (1,000 years) simulations of the Geophysical Fluid Dynamic Laboratory (GFDL) - CM2.1 Earth System Model (ESM) fully coupled with the marine ecosystem model TOPAZv2 (Tracers of Ocean Phytoplankton with Allometric Zooplankton Version 2; Dunne et al., 2013).

Additionally, in the revised manuscript, we assessed the relative contributions of three mechanisms using a regression method instead of the joint-composite analyses (Figure R7, Table R1; We added Figure R7 and Table R1 as Figure 9 and Table 1 in the manuscript respectively). We normalized all variables and conducted multiple regression for three mechanism indices at each grid point of SCHL anomalies across the target region. And, we quantified the relative contributions of three mechanisms by multiplying the linear regression coefficients between the Nino3.4 index and each mechanism index by their multiple regression coefficients respectively (Eq. 1; We added it as Eq. 4 in the manuscript).

The results indicate that both the Runoff- and the TS-transport-driven mechanism have the most significant contributions to the intensity of SCHL blooming in the target region. Although the Ekman Upwelling-driven mechanism exhibits a lower contribution compared to the others, it still exerts a meaningful influence on about half of the other mechanisms. Spatially, the Runoff-driven mechanism primarily affects the central area of the target region (Figure R7a), while the TS-transport-driven mechanism plays a major role along a southwest-northeast diagonally (Figure R7b). In contrast, the Ekman Upwelling-driven mechanism uniformly influences the overall target region (Figure R7c). Especially, the runoff- and the TS-transport-driven mechanism contribute similarly to the SCHL blooming intensity in the target region. Although the Ekman upwelling-driven mechanism accounts for approximately 40 to 47% of the others, it still exerts a significant influence (Table R1). Consequently, we

have replaced the paragraph that calculated the relative contribution for each mechanism from the joint-composite analyses previously we used to the regression method as follows:

(L313-349): So far, we have conducted a comprehensive evaluation and analysis of the complex mechanisms driving phytoplankton blooms in the ECS during the summers following the decaying phase of El Niño events. In addition to the runoff- and TS-transport-driven mechanisms suggested in previous studies, we introduced the Ekman upwelling-driven blooming mechanism. Subsequently, we quantified the relative contributions of these three mechanisms based on regression methods using (Eq. 4) as follows:

$$\frac{dChl}{dNino3.4}(\alpha) = \frac{\partial Chl}{\partial Runoff} \times \frac{dRunoff}{dNino3.4} + \frac{\partial Chl}{\partial TS-transport} \times \frac{dTS-transport}{dNino3.4} + \frac{\partial Chl}{\partial Ekman-Upwelling} \times \frac{dEkman-Upwelling}{dNino3.4} + residual \quad (4)$$

Firstly, we normalized all variables and conducted the multiple regression with respect to SCHL index in the target region as the dependent variable and three mechanism indices as independent variables. Secondly, we calculated each term by multiplying the linear regreesion coefficient between Nino3.4 index and each mechanism index by the corresponding multiple regression coefficient for each mechanism index. The combined effects of the three mechanisms and the residual term collectively account for the variation of the SCHL index in the ECS region with respect to the El Niño events. Therefore, each term indicates how changes in three mechanism induced by ENSO cycle (as indicated by the Nino3.4 index) affect on phytoplankton blooms in the ECS region. The results show the effect of runoff-driven mechanism and the TS-transport mechanisms to SCHL blooming intensity in the target region are comparable (Table 1). In the case of the Ekman upwelling mechanism, it accounts for about 40% to 47% of contributions comapred to the other two mechanisms, yet still exerts a meaningful influence as well.

Table R1. Relative contributions of three mechanisms to SCHL blooming in the target region.

	α	Runoff	TS-transport	Ekman Upwelling
Contribution	0.511	0.152	0.138	0.065

Additionally, we identified their spatial contributions to further elucidate the effects of each mechanism within the target region (Figure 9). We conducted multiple regression for three mechanism indices at each grid point of SCHL anomalies across the target region. Following the same way examined above, we calculated the spatial contributions by multiplying the linear regression coefficents of each mechanism with repsect to the Nino3.4 index. The results showed that the runoff-driven mechanism exhibited the strongest contribution at the center of the target region, driven by direct riverine nutrient inflow (though the model doesn't simulate P input) and nutrient supply through buoyancy upwelling induced by river discharge (Figure 9a). In contrast, the TS-transport-driven mechanism significantly contributes along a southwest-northeast diagonal direction, aligning with nutrient transport via the TS from the SCS (Figure 9b). Additionally, the newly proposed Ekman upwelling-driven mechanism, while relatively lower in overall contribution, shows significant and uniformly distributed impacts across the target region (Figure 9c). These results suggest that all mechanisms can affect comprehensively to induce phytoplankton blooms in the ECS during the following summers of the decaying phase of El Niño events. Therefore, considering all mechanisms is essential for accurately predicting the intensity of phytoplankton blooms.

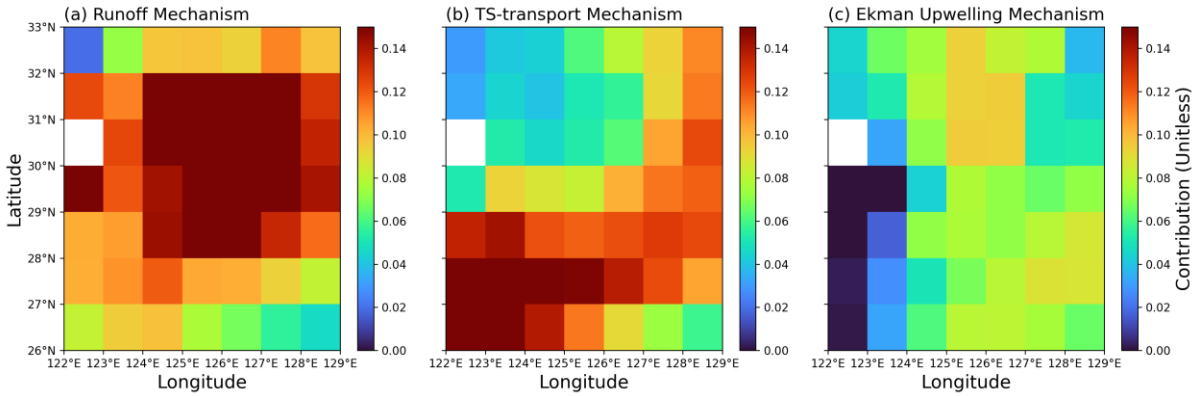

Figure R7. Relative contributions of three mechanisms to SCHL blooming in the target region during summers following the decaying phase of El Niño events **(a)** Runoff-driven mechanism **(b)** TS-transport-driven mechanism **(c)** Ekman upwelling-driven mechanism.

• In describing the TOPAZ model, the authors stated Dunne et al. (2010, 2013) TOPAZ model is implemented in this study. As TOPAZ is developed in completely different context. I am not sure if the authors have done anything to tune the model parameters for ECS regions? If so, the model parameters should be listed in a table, if not in the main texts, should be in supplementary materials.

Response: We conducted the experiments using the GFDL-CM2.1 Earth System Model coupled with the TOPAZ biogeochemical model, but we did not make any adjustments or tuning of model parameters.

• English is mostly well written, but therse are places where comprehension is compromised due to incorrect English.

Response: Thank you for your comments on the English writing. We tried to improve the English description and expressions throughout the entire manuscript.

Detailed comments:

• Line 39: citation of Racault et al. (2017) is not appropriate, as that paper does not address ECS specifically.

Response: We have corrected with more appropriate references.

• Line 42: What does YECS stand for?

Response: Sorry for omitting the abbreviation. We have revised it in the manuscript as follows:

(L44) “Yellow and East China Seas (YECS)”

• Line 89: Fe is a ”micronutrients”, but others are macronutrients.

Response: We have revised it in the manuscript for clarify as follows:

(L102) “macronutrients & micronutrients”

• Figure 1: How were the anomalies calculated? Are they against annual mean? or a climatology of certain period? Need to be precisely stated.

Response: We have added the description of the anomaly as follows:

(L104-105) “All anomalies are calculated by removing the seasonal cycles and the linear trend.”

• Line 102: Yamaguchi et al. (Year?)

Response: Corrected.

(L117) “Yamaguchi et al (2012)”

• Line 113-114: “This anomalous phytoplankton bloom during the boreal summer season of the following El Niño events has been explained by enhanced precipitation.” This sentence is hard to read. Are you trying to say the anomalous phytoplankton bloom following the El Nino events has been explained by enhanced precipitation?

Response: In order to address the aims of our study and improve readability, we have revised the manuscript as follows:

(L132-135) “The anomalous phytoplankton blooms during the summers following El Niño events can be attributed to increased riverine discharge from the YR, driven by enhanced precipitation, and the substantial nutrient supply through the TS from the South China Sea (SCS).”

• Figure 2(e, and f): What do red and red squares stand for? Describe it in the legend.

Response: The red and blue squares represent the YRE and Extended YRE regions, respectively, and we have added the description to the Figure 2 caption.

• Figure 4a: What are the gray dots for?

Response: Figure 4a shows the relationship between the Nino3.4 DJF index and area-averaged surface chlorophyll-a anomalies over the target region in GFDL-CM2.1 ESM used in the research. Gray dots represent the non-El Niño cases. We have added the description of the gray dots in Figure 4 caption.

• Line 173-174: Where is the observed patterns of NO3 and PO4?

Response: Annual nutrient distribution from World Ocean Atlas (WOA) reanalysis data reveals a NO_3-dominated pattern centered around the YRE, which is attributable to strong river discharge. In contrast, PO_4 concentrations remain relatively low throughout the entire ECS region.

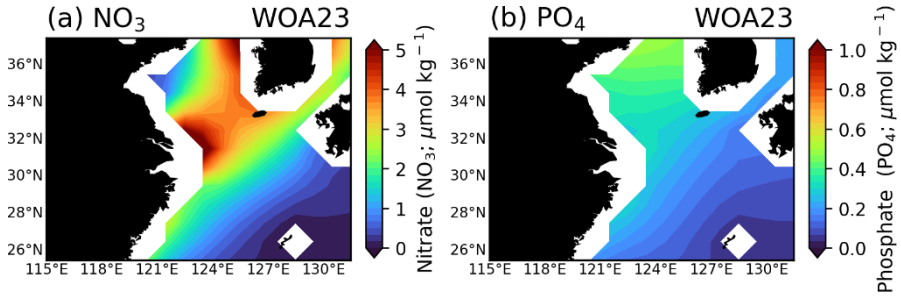

Figure R8. Annual mean nutrient distribution **(a)** NO3 **(b)** PO4 concentrations

• Fig. 5: How did you simulate runoff? It appears there is no grid close to the coast due to coarse resolution.

Response: The model simulates the runoff in the grids where dots are displayed in Figure 5d-f.

• Line 260: " within the red box in Fig. 7g". The red box is in Fig. 7c.

Response: Corrected.

• Line 261-263: How deep could be the upwelling, and what is the nutrient concentration of the upwelling horizon?

Response: The ECS is featured by shallow waters, with a maximum depth of

approximately 50 meters, making it highly conducive to the upward transport of nutrients from the subsurface layer through upwelling.

Jing et al (2009) mentioned that the local winds in the northern coastal region of the South China Sea can induce upwelling within 100m depth of water column. This suggests that such upwelling is sufficient to transport nutrients to the surface layer, promoting the growth of phytoplankton and enhancing primary productivity in the ECS region.

• Line 274: “Joint composition analysis” may not be familiar to large number of readers, including myself. A reference should be provided.

Response: In the revised manuscript, we assessed the relative contributions of three mechanisms using a regression method instead of the joint-composite analyses.

Therefore, we have replaced the paragraph that calculated the relative contribution for each mechanism from the joint-composite analyses to the regression method.

• Fig 9(a) and Fig 7(a-c): The position of modelled and observed position of GPH anomalies are quite different in latitude. Need some explanations.

Response: Figures 7a–c show the location of the WNPAC in the model results. During the summer of the El Niño decaying phase, the WNPAC location in the observations (16.5°N–26.5°N / 130°E–155°E) and the model (13.5°N–26.5°N / 124.5°E–160.5°E) are slightly different in terms of zonal location.

We have added a description of the location of the WNPAC index in the model results shown in Figure 8c as the red box in the revised manuscript:

(L307-309) “The correlation between WSCL and the WNPAC index (13.5°N–26.5°N / 124.5°E–160.5°E; which is slightly broader than observations) calculated from GPH anomalies within the red box in Fig. 8c exhibits a significantly positive relationship (r =

0.45**) at the 99% confidence level"

• Line 368: What do you mean by "two seasons"?

Response: It refers to the El Niño peak phase (D(0)JF(1)), which represents two seasons prior to the El Niño decaying summers (JJA(1))

• Lines 370-371: Not clear about the correlation between what? Do you mean the correlation between observation and ESM results?

Response: Figures 11a–d illustrate the lagged relationship between the WNPAC index and observed SCHL concentration for the D(0)JF(1)–JJA(1) in Figure 11a-b and MAM(1)–JJA(1) in Figure 11c-d in observations. Figures 11e–h present the correlations between model results as same as Figure 11a-d. To prevent confusion between observations and models in Figure 11 (previously Figure 10 in the manuscript), we have added the additional explanation as follows:

(L421-422) "We found a significantly positive lagged relationship between the WNPAC index and blooming magnitude in the ECS region in both observations and ESM results (Figure 11a-d; Observations, Figure 11e-h; Model)."

Reference

Chen, C. T. A., Yeh, Y. T., Chen, Y. C., and Huang, T. H.: Seasonal and ENSO-related interannual variability of subsurface fronts separating West Philippine Sea waters from South China Sea waters near the Luzon Strait, Deep. Res. Part I Oceanogr. Res. Pap., 103, 13–23, https://doi.org/10.1016/j.dsr.2015.05.002, 2015.

Dunne, J., Gnanadesikan, A., Sarmiento, J. L., and Slater, R. D.: Technical description of the prototype version (v0) of Tracers Of Phytoplankton with Allometric Zooplankton (TOPAZ) ocean biogeochemical model as used in the Princeton IFMIP* model, Biogeosciences, 7, 3593, 2010.

Dunne, J. P., John, J. G., Shevliakova, E., Stouffer, R. J., Krasting, J. P., Malyshev, S. L., Milly, P. C. D., Sentman, L. T., Adcroft, A. J., Cooke, W., Dunne, K. A., Griffies, S. M., Hallberg, R. W., Harrison, M. J., Levy, H., Wittenberg, A. T., Phillips, P. J., and Zadeh, N.: GFDL's ESM2 Global Coupled Climate–Carbon Earth System Models. Part II: Carbon System Formulation and Baseline Simulation Characteristics*, J. Clim., 26, 2247–2267, https://doi.org/10.1175/JCLI-D-12-00150.1, 2013.

Huang, T. H., Chen, C. T. A., Zhang, W. Z., and Zhuang, X. F.: Varying intensity of Kuroshio intrusion into Southeast Taiwan Strait during ENSO events, Cont. Shelf Res., 103, 79–87, https://doi.org/10.1016/j.csr.2015.04.021, 2015.

Jing, Z. you, Qi, Y. quan, Hua, Z. lin, and Zhang, H.: Numerical study on the summer upwelling system in the northern continental shelf of the South China Sea, Cont. Shelf Res., 29, 467–478, https://doi.org/10.1016/j.csr.2008.11.008, 2009.

Yamaguchi, H., Kim, H. C., Son, Y. B., Kim, S. W., Okamura, K., Kiyomoto, Y., and Ishizaka, J.: Seasonal and summer interannual variations of SeaWiFS chlorophyll a in the Yellow Sea and East China Sea, Prog. Oceanogr., 105, 22–29, https://doi.org/10.1016/j.pocean.2012.04.004, 2012.

Zhang, W., Zhuang, X., Chen, C. A., and Huang, T.: The impact of Kuroshio water on the source water of the southeastern Taiwan Strait: numerical results, Acta Oceanol. Sin., 34, 23–34, https://doi.org/10.1007/s13131-015-0720-x, 2015.